KRIGING, OPTIMAL SAMPLING AND FILTERING BY KRIGING ANALYSIS

Third Interim Report (RSSUSA - 2/3)

Dr Margaret A. Oliver and Professor Richard Webster

May 1996 to July 1996

United States Army

ENVIRONMENTAL RESEARCH OFFICE OF THE U.S. ARMY

London, England

CONTRACT NUMBER - N68171 - 95 - C - 9128

REPORT DOCUMENTATION PAGE

Form Approved
OMB No. 0704-0188

1. AGENCY USE ONLY (Leave blank)	2. REPORT DATE	3. REPORT TYPE AND DATES COVERED
	20. 08. 96	Interim – May 1996 - July 1996

4. TITLE AND SUBTITLE
Optimal sampling, ordinary kriging and kriging analysis for filtering of the remote imagery for Fort Benning

5. FUNDING NUMBERS
N68171-95-C-9128

6. AUTHOR(S)
Dr Margaret A. Oliver, Professor Richard Webster

7. PERFORMING ORGANIZATION NAME(S) AND ADDRESS(ES)
University of Reading, Whiteknights,
Reading, RG6 6AH, UK.

8. PERFORMING ORGANIZATION REPORT NUMBER
(RSSUSA - 2/3)

9. SPONSORING/MONITORING AGENCY NAME(S) AND ADDRESS(ES)
USARDSG-UK, Environmental Sciences Branch,
Edison House, 233 Old Marylebone Road,
London, NW1 5TH, UK.

10. SPONSORING/MONITORING AGENCY REPORT NUMBER

11. SUPPLEMENTARY NOTES
Mapping and filtering of the Fort Benning image data by kriging.

12a. DISTRIBUTION/AVAILABILITY STATEMENT
No limitation on distribution/availability

12b. DISTRIBUTION CODE

13. ABSTRACT (Maximum 200 words)

This is the third report on the second phase of the project to apply geostatistics to remote imagery. The main focus of this period of work has been to apply the geostatistical technique of kriging to the image information for Fort Benning in different ways. The first section describes how the kriging equations can be used to optimize sampling effort. The results of this will relate to the last phase of work for this contract on data compression. They show how the estimation variance increases as the grid spacing increases or the number of data retained decreases. Ordinary kriging was used to map the data for Channels 2, 3 and NDVI to produce contour maps. The aim eventually is to assess how well the categories in these maps reflect the different classes of ground cover. The image data were finally filtered by kriging the long and the short range components in the vegetation. The maps of the short range component show the local rate of change in the pattern of ground cover while those of the long range component show the extent of the major patches of different kinds of ground cover.

14. SUBJECT TERMS	15. NUMBER OF PAGES
Fort Benning, filtering, kriging, optimal sampling, short range component, long range component.	16. PRICE CODE

17. SECURITY CLASSIFICATION OF REPORT	18. SECURITY CLASSIFICATION OF THIS PAGE	19. SECURITY CLASSIFICATION OF ABSTRACT	20. LIMITATION OF ABSTRACT

NSN 7540-01-280-5500

Standard Form 298 (Rev 2-89)
Prescribed by ANSI Std Z39-18
298-102

ATTACHMENT 1
PAGE 1 OF 2

ABSTRACT

This is the third report on the second phase of the project to apply geostatistics to remote imagery. We have applied different aspects of kriging to the image information for Fort Benning. The first section describes how the kriging equations were used to optimize sampling effort. The results show how the estimation variance increases as the grid spacing increases or the number of data retained decreases. This will have implications for the last phase of work for this contract on data compression. Ordinary kriging was used to map the data for Channels 2 and 3 and NDVI to produce contour maps. The aim eventually is to assess how well these maps reflect the different classes of ground cover. The image data were finally filtered by kriging the long- and the short-range components in the ground cover. The maps of the short-range component show the local change in the pattern of ground cover while those of the long range component show the extent of the major patches of different kinds of the cover.

INTRODUCTION

This report covers an investigation to explore kriging of the SPOT image for the part of Fort the Benning being studied. First we describe kriging and how it has been used to show the likely estimation variances for different sampling intensities in relation to the three wavebands. The kriging equations enable sampling schemes to be designed when the variogram is known and before collecting any data. The pixel values for channels 2 (Red, R), 3 (Infra-red, I) and for the normalized difference vegetation index, NDVI = (I - R)/(I + R), were also kriged to obtain a choropleth map. The aim of kriging pixel data is twofold: to remove some of the noise from the image and to remap the information based on isarithms chosen to match the likely reflectance of the vegetation. A more effective way of removing noise than ordinary kriging is to filter the pixel information by a kriging analysis. In the previous project we detected two marked scales of spatial variation in the image from the variogram analysis. The variogram showed that there was a short-range variation of about 9 pixels long (180 m) and a much longer one of about 150 pixels (3 km). We filtered the image according to these spatial scales by kriging the short and the long spatial components independently.

The theory of kriging and its relation to optimal sampling is described, and the theory of the kriging analysis to filter data is also given.

GEOSTATISTICAL THEORY

In geostatistics the values $z_u(\mathbf{x})$ of any variable, u, distributed in space are regarded as constituting a particular realization of a random variable $Z_u(\mathbf{x})$, where $(\mathbf{x})$ denotes the spatial co-ordinates in one, two or three dimensions. The random variable is usually autocorrelated at some scale, and it may be correlated with one or more other random variables, $v, \ldots,$. Characterizing the variable and analysing measurements

of it build more or less elaborately on this basic assumption. For the present purpose we confine ourselves to linear models. Further, each variable is treated independently in this study.

Linear model.

We assume a simple model of a spatially correlated random variable:

$$Z(\mathbf{x}) = \mu + \varepsilon(\mathbf{x}) , \tag{1}$$

where μ is the mean of the process, and $\varepsilon(\mathbf{x})$ is another random variable with a mean of zero and variogram $\gamma(\mathbf{h})$ where $\mathbf{h}$ is the lag.

If we assume the intrinsic hypothesis, namely that the expected differences between the values at $\mathbf{x}$ and $\mathbf{x}+\mathbf{h}$ is 0 and their variance depends only on $\mathbf{h}$ then $\gamma(\mathbf{h})$ is also the variogram of $Z(\mathbf{x})$.

Characteristics of kriging

At its simplest kriging is a method of local weighted moving averaging of the observed values within a neighbourhood V. Weights are allocated to the sample data within the neighbourhood of the point or block to be estimated. The weights depend on the structure of the variation of the property, defined by the variogram model, and the configuration of the sampling sites. The weights are allocated so as to minimize the estimation variance, or kriging variance, and the estimates are unbiased. Hence, in this sense, kriging is an optimal estimator. Kriging is also an exact interpolator in the sense that the kriged value at a sampling site is the observed value there, and the estimation variance is zero. Kriging can be done at points or over areas (blocks). In the analysis that we report here we regarded each pixel in the image from Fort Benning as a point and used punctual kriging.

Theory of Linear kriging

In the usual situation a kriged estimate, $\widehat{Z}(\mathbf{x}_0)$, is a weighted average of data, $z(\mathbf{x}_1), z(\mathbf{x}_2), \ldots, z(\mathbf{x}_N)$:

$$\widehat{Z}(\mathbf{x}_0) = \sum_{i=1}^{N} \lambda_i z(\mathbf{x}_i) , \tag{2}$$

where λ_i are the weights.
To ensure that the estimates are unbiased the weights are made to sum to 1:

$$\sum_{i=1}^{N} \lambda_i z(\mathbf{x}_i) = 1 .$$

We also want to minimize the estimation variance, which is given by

$$\begin{aligned} \mathrm{var}[\widehat{Z}(\mathbf{x}_0)] &= \mathrm{E}[\{\widehat{Z}(\mathbf{x}_0) - Z(\mathbf{x}_0)\}^2] \\ &= 2\sum_{i=1}^{N} \lambda_i \gamma(\mathbf{x}_i, \mathbf{x}_0) - \sum_{i=1}^{N}\sum_{i=j}^{N} \lambda_i \lambda_j \gamma(\mathbf{x}_i, \mathbf{x}_j) , \end{aligned} \tag{3}$$

where $\gamma(\mathbf{x}_i, \mathbf{x}_j)$ is the semivariance of Z between points $\mathbf{x}_i$ and $\mathbf{x}_j$, and $\gamma(\mathbf{x}_i, \mathbf{x}_0)$ is the semivariance between the ith datum and the point for which the estimate is required.

In ordinary kriging the mean of the random variable, μ, is unknown. The estimation variance of $Z(\mathbf{x}_0)$ is minimized, subject to the non-bias condition, when

$$\begin{aligned} \sum_{i=1}^{N} \lambda_i \gamma(\mathbf{x}_i, \mathbf{x}_j) + \psi(\mathbf{x}_0) &= \gamma(\mathbf{x}_j, \mathbf{x}_0) \text{ for all } j \\ \sum_{i=1}^{N} \lambda_i \gamma(\mathbf{x}_i) &= 1 . \end{aligned} \tag{4}$$

These are the kriging equations. The quantity $\psi(\mathbf{x}_0)$ is a Lagrange multiplier, which is introduced to achieve the minimization. The kriging variance is then obtained from

$$\sigma_e^2 = \sum_{i=1}^{N} \lambda_i \gamma(\mathbf{x}_i, \mathbf{x}_0) + \psi(\mathbf{x}_0) . \tag{5}$$

OPTIMAL SAMPLING

The estimation variance for kriging depends only on the variogram and the configuration of sampling points and not on the measured values. This means that if the variogram is known then the estimation variances can be determined for any desired sampling configuration *before* the sampling is done. Therefore, we should be able to design a sampling scheme to meet a specified tolerance or precision for a property. We may or may not have data at this stage. In this case we had the image data, but for field work or to sample the image for data compression we want to minimize the ground-based sampling or the number of data retained according to the estimation variance (the square of the standard error) that we can tolerate.

We determined the models for the variograms previously. They were all isotropic double exponential, with equation

$$\gamma(\mathbf{h}) = c_0 + c_1\{1 - \exp(-h/a_1)\} + c_2\{1 - \exp(-h/a_2)\} , \tag{6}$$

in which c_0 is the nugget variance, c_1 and c_2 are the sills of the short-range and long-range components respectively, and a_1 and a_2 are the corresponding distance parameters. The values of the parameters are given in Table 1. Using these models we formed the punctual kriging system, Equations (4), and solved it to determine the punctual kriging variances by Equation (5) at the centres of grid cells for grid sizes of 4, 8, ...,. These are the largest variances associated with the reconstruction of the images from sampling at the intervals 4, 8, ...,.

One might wish to discover the minimum number of pixels to retain and still maintain a sufficiently small error, an acceptable tolerance. For this we plotted the

Table 1: Variogram model parameters for the three channels and NDVI

Channel	c_0 variance	c_1 variance	c_2 variance	a_1 pixels	a_2 pixels
1 – rows	0	35.74	43.95	2.83	28.61
– columns	0.88	44.92	45.92	3.76	61.67
– average	0	40.84	42.71	3.26	38.87
2 – rows	0	0.0213	0.0904	2.19	44.67
– columns	0	0.0329	0.0854	4.49	79.00
– average	0	0.0262	0.0845	3.23	53.36
3 – rows	0	0.0105	0.0467	1.76	52.91
– columns	0	0.0130	0.0335	3.03	52.47
– average	0	0.0115	0.0400	2.33	51.92
NDVI					
– rows	0	0.00406	0.00942	4.51	70.45
– columns	0	0.00422	0.00569	5.24	38.85
– average	0	0.00428	0.00725	5.06	55.80

NB The distance parameters of the variograms can be multiplied by 3 to obtain the approximate range of spatial dependence.

estimation variances against grid spacing for the three wavebands, Figure 1, from which the sample spacing can be read for any specific tolerance.

We do not know what error is tolerable in this instance. Nevertheless, from the graphs it is clear how the estimation variance increases rapidly with increased sample spacing, or equivalently a smaller sample. For data compression, which we shall deal with in the final report, the graphs illustrate at the outset the kind of estimation variances or standard errors we shall incur by removing information.

Results of optimal sampling analysis

Channel 1

The graph of the estimation variances plotted against grid spacing in numbers of pixels for channel 1 has a very steep initial slope. This results from the short-range component of the variogram. The pixel map of channel 1 shows that the short range variation is dominant. If a variance of 50 is chosen for the tolerance, which is 62.5% of the upper limit of the variance in this graph, then a sampling interval of 9 pixels

would be needed. Hence, estimates based on this sampling interval would have a considerable error even though the sampling interval or reduction in data would be fairly small. For the vegetation survey in the previous project we recommended a minimum sampling interval of 150 m (7.5 pixels) which would give an estimation variance of about 38, about 50% of the total variance. With a sampling interval of more than 60 pixels (1500 m) for channel 1, which was the maximum sampling interval, we recommended for sampling the long-range component there would be little spatial dependence in the data. This graph confirms our earlier recommendations. It also shows the importance of an objective approach to sampling for interpolation or data reduction.

Channel 2

The initial slope of this graph is also steep. Later it becomes more gradual. The variances this time are for the data transformed to logarithms. This suggests that the short- and long-range components are both important for this waveband. The pixel map of this channel appears less noisy than that of channel 1. For a spacing of 7.5 pixels the estimation variance would be 30%, and for one of 45 pixels 60%.

Channel 3

This graph has the gentlest slope, although it is still steep near to the origin arising from the short-range component of the variation. A sampling interval of 7.5 pixels would result in an estimation variance of 30% of the total, whereas for a 50-pixel sampling interval it would be 60% for the long-range component.

Channels 2 and 3 (Red and Near Infra Red) are the ones we expect to be most closely related to the vegetation. They are also similar to each other and express a similar degree of variation.

Summary

Figure 1 shows the maximum estimation variances that would result when reconstructing images from sampling the image for data reduction. Clearly it depends on the variation in the data. These graphs also show the effect of the two scales of variation on the sampling interval needed to resolve the variation present.

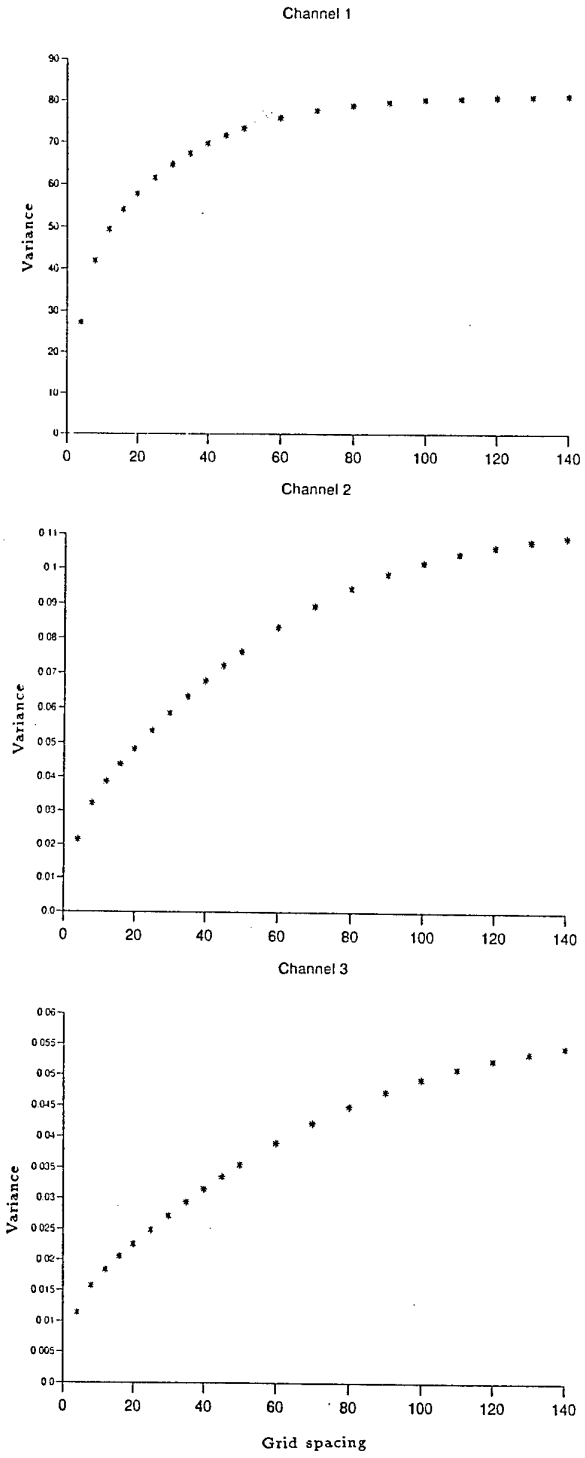

Figure 1: Graphs of estimation variance against sampling interval for Channel 1 (Green); Channel 2 (Red) and Channel 3 (Infra-red).

KRIGING

For this part of the project we have been examining the best way of smoothing or removing noise from the pixel information for mapping. The simplest approach was to use ordinary kriging for the reflectance values of channels 2 and 3 and for NDVI (the standardized vegetation index). We used the double exponential model of the raw data for each to these variables and kriged the raw data on a grid that was offset by 0.5 of a pixel in both the north-south and east-west dimensions; this was to avoid estimating at the data points, which would have been useless. We used the raw data so that TEC can make comparisons between the isarithmic intervals and the reflectance values for the classes of vegetation. We kriged both at intervals of 1 and 2 pixels. We drew only the maps of the latter estimates because there was little benefit in using the more detailed estimates.

For kriging we had to subdivide the area because of its irregular shape. With such a fine grid we had large areas in the rectangle that were blank, and no estimates were produced for the bottom third of the study area. In this report the maps of the top part of the image are included, although the others have been made available to Mr Slocum.

Results of ordinary kriging

For channels 2 and 3 (R and I, respectively), Figures 2 a and 3 a, the isarithmic intervals were chosen to correspond with the average reflectance for the different classes of vegetation suggested by TEC. This was more straightforward for channel 2 because the spectral values seemed to match those of the vegetation closely. This waveband also had the largest correlation with the vegetation values when they were compared in the previous project. The reflectance values associated with the ground cover classes for Channel 2 are given in Table 2.

The general appearance of the maps for Channels 2 and 3 is similar, especially for the large reflectance values over the open spaces and roads. The major differences in the pattern are in the south west. Here there appear to be differences in the short-range variation picked up by the different sensors. In both cases the swampy areas associated with the Ochillee Creek show up clearly with the blue shading. Also Kings Pond is clearly visible on both maps (Figures 2 a and 3 a).

The map for NDVI (Figure 4 a) is somewhat different from the others: the high reflectance areas (small NDVI) are more clearly defined. It appears to contain more detail of the variation. The map is more similar to that of Channel 3 than that of the other channels, suggesting that NDVI reflects the pattern in the Infra-red more than in the red, even though it is slight. This is more apparent in the kriged maps of the southern part of the region, Figures 2 b, 3 b and 4 b. For Channel 3 and NDVI the western and eastern halves of the map appear very different. This distinction is also present further North, but it is less clear. It seems to follow the physiography, with the boundary following more or less the western edge of the Branch valley.

In all of the kriged maps the short- and long-range components of the variation are clearly visible. These maps need to be validated now against the field data

Table 2: Average reflectance values associated with ground cover class for channel 2

Ground cover class	Reflectance Value
Water	24.0
Pine/Hardwood Wet	25.0
Hardwood/Pine Wet	25.9
Brush	26.1
Pine/Hardwood	26.3
Hardwood Wet	26.5
Pine/Plantation	27
Longleaf Pine	28
Oak/Pine	29
Open space	30

that were collected in the Autumn of 1995 by TEC. We did not have these data available for comparison. The next stage is for the team at TEC to compare the kriged maps with the ones of the classification of ground cover to see which is better for predicting ground cover.

KRIGING ANALYSIS

The variogram may be just one simple structure, or it may be the sum of two or more structures, one nested inside the other, and each with its own scale, thus

$$\gamma(\mathbf{h}) = \gamma^1(\mathbf{h}) + \gamma^2(\mathbf{h}) \dots , \tag{7}$$

where the superscripts refer to the separate structures. This matches the real world in which factors such as relief, geology, tree-throw, fauna, and man's divisions into fields and farms operate on their own characteristic scales.

If we assume that the pocesses are uncorrelated then we can represent Equation (2) by the sum of K basic variograms:

$$\gamma(\mathbf{h}) = \sum_{k=1}^{K} b^k g^k(\mathbf{h}) , \tag{8}$$

where $g^k(\mathbf{h})$ is the kth basic variogram function and b^k is a coefficient that measures the relative contribution of $g^k(\mathbf{h})$ to the sum. This then is our linear model of regionalization.

Identifying the spatial structures.

Working from sufficient data we can attempt to identify the separate spatial structures. We first compute the experimental variogram, for which the usual estimator is

$$\widehat{\gamma}(\mathbf{h}) \;=\; \frac{1}{2m(\mathbf{h})} \sum_{i=1}^{m(\mathbf{h})} \{z(\mathbf{x}_i) - z(\mathbf{x}_i + \mathbf{h})\}^2 \;, \tag{9}$$

where $z(\mathbf{x_i})$ and $z(\mathbf{x} + \mathbf{h})$ are observed values of Z, and $m(\mathbf{h})$ is the number of paired comparisons at lag $\mathbf{h}$. Changing $\mathbf{h}$ gives the experimental variogram, to which must be fitted a legitimate variogram function. In practice, we find that most experimental variograms require a nested model to describe them accurately and that we do have to combine two or more basic functions, as in Equations (7) and (8). The nested model we used below includes two exponential functions, Equation (6), but without the nugget.

Kriging analysis.

Once distinct spatial structures have been identified in the variogram we can try to separate their sources. This is effectively filtering. It enables us to isolate specifically local or regional sources of variation and, thereby, interpret them more easily than when they are combined. For image data which are complex separating out the different sources of variation helps to show the spatial structure present at the different scales, and it reduces the noise. It is done by what Matheron (1982) called 'kriging analysis', and it is based on the decomposition of $Z(\mathbf{x})$ into the sum if K separate orthogonal random functions $Z^k(\mathbf{x}), k = 1, 2, \ldots, K$, each with its basic variogram $g^k(\mathbf{h})$ of Equation (8):

$$Z(\mathbf{x}) \;=\; \sum_{k=1}^{K} Z^k(\mathbf{x}) + \mu \;, \tag{10}$$

such that

$$\mathrm{E}[Z^k(\mathbf{x})] \;=\; 0$$

and

$$\begin{aligned} \frac{1}{2}\mathrm{E}[\{Z^k(\mathbf{x}) - Z^k(\mathbf{x}+\mathbf{h})\}\{Z^{k'}(\mathbf{x} - Z^{k'}(\mathbf{x}+\mathbf{h})\}] \;&=\; b^k g^k(\mathbf{h}) \quad \text{if} \quad k = k' \\ &=\; 0 \quad \text{otherwise} \;. \end{aligned} \tag{11}$$

Relation (11) expresses the mutual independence of the K random functions $Z^k(\mathbf{x})$. With this assumption, the nested model (8) is easily retrieved from relation (10). We assume that $Z(\mathbf{x})$ is second-order stationary, which accords with the results above. The $Z^k(\mathbf{x})$ are the spatial components, and they represent the behaviour of $Z(\mathbf{x})$ at the spatial scales defined by the distance parameters of the basic

variogram functions, $g^k(\mathbf{h})$. In practice each spatial component is estimated as a linear combination of the observations $z(\mathbf{x}_i)$:

$$\widehat{Z}^k(\mathbf{x}_0) = \sum_{i=1}^{n} \lambda_i^k z(\mathbf{x}_i) , \tag{12}$$

where n is the number of observations, $z(\mathbf{x}_i), i = 1, 2, \ldots, n$, used for the estimation, and the λ_i^k are the weights assigned to the observations.

The n weights are chosen to ensure that the estimate is unbiased and that the estimation variance is minimal. This leads to the kriging system:

$$\begin{aligned} \sum_{j=1}^{n} \lambda_j^k \gamma(\mathbf{x}_i, \mathbf{x}_j) - \psi &= b^k g^k(\mathbf{x}_i, \mathbf{x}_0) \quad \text{for all} \quad i = 1, 2, \ldots, n , \\ \sum_{j=1}^{n} \lambda_j^k &= 0 . \end{aligned} \tag{13}$$

This system is is solved to find the weights, λ_i^k, to insert into Equation (12). The quantity ψ is a Langrange multiplier. From Equation (10), $\mathrm{E}[Z^k(\mathbf{x})] = \mathbf{0}$, and so the weights sum to 0 to assure unbiasedness, not to 1 as in the ordinary kriging formulation, system (4).

To account for local non-stationarity the kriging is usually done in fairly small moving neighbourhoods centred on $\mathbf{x}_0$. Then it is necessary only that $Z(\mathbf{x})$ is locally stationary, or *quasi-stationary*, so that Equation (10) can be rewritten as

$$Z(\mathbf{x}) = \sum_{k=1}^{K} Z^k(\mathbf{x}) + \mu(\mathbf{x}) , \tag{14}$$

where $\mu(\mathbf{x})$ is a local mean which can be considered as a long-range spatial component. Matheron (1982) has shown that this relation is also verified in terms of estimators, i.e.

$$\widehat{Z}(\mathbf{x}) = \sum_{k=1}^{K} \widehat{Z}^k(\mathbf{x}) + \widehat{\mu}(\mathbf{x}) . \tag{15}$$

The local mean is estimated as a linear combination of the observations $z(\mathbf{x}_i)$:

$$\widehat{\mu}(\mathbf{x}_0) = \sum_{j=1}^{n} \lambda_j z(\mathbf{x}_j) . \tag{16}$$

The weights are obtained by solving the kriging system:

$$\begin{aligned} \sum_{j=1}^{n} \lambda_j \gamma(\mathbf{x}_i, \mathbf{x}_i) - \psi &= 0 \quad \text{for all} \quad i = 1, 2, \ldots, n , \\ \sum_{j=1}^{n} \lambda_j &= 0 . \end{aligned} \tag{17}$$

Estimation of the long-range component, i.e. the local mean $\mu(\mathbf{x})$ and the spatial component with the largest range, can be affected by the size of the moving neighbourhood, see Galli *et al.* (1984). In fact, to estimate a spatial component with a given range, the diameter of the neighbourhood should be at least equal to that range. It frequently happens when the sampling density and the range are large that there are so many data within the chosen neighbourhood that only a small proportion of them is retained. Although modern computers can handle many data at a time, the number of data used must be limited to avoid instabilities when inverting very large covariance matrices. Further, even if all the data could be retained, only the nearest ones contribute to the estimate because they screen the more distant data. Consequently, the neighbourhood actually used is smaller than the neighbourhood specified, which means that the range of the estimated spatial component is smaller than the range apparent from the structural analysis. Galli *et al.* (1984) recognized this, and where data lie on a regular grid they proposed using only every second or every fourth point to cover a large enough area but still with sufficient data. Such selection is somewhat arbitrary, and we have adopted an alternative proposed by Jaquet (1989) which involves adding to the long-range spatial component the estimate of the local mean.

Results of the kriging analysis: filtering

Short range

For Channel 2 (R), Figure 2 c, the detailed local variation associated with erosion in the area of McKenna Hill shows clearly. This area has large reflectance values because it has been cleared of vegetation. The roads are also distinct, as are the other areas that have been cleared. The short-range variation in the vegetation is also evident. There appear to be two main classes of reflectance, but this depends to some extent on the class intervals chosen. Essentially this map shows the main local changes and where these can be expected from one ground cover class to another. It is not possible to say what the type of cover is from this map at present.

The map, Figure 3 c, for Channel 3 (I) shows more detail in the short-range variation. However, McKenna Hill does not stand out as clearly. There are now three main reflectance groups in the vegetation. We need to discuss these maps with Mr Slocum to discover their meaning. What is apparent is that the swamp in the southern central part of the image is not evident at this scale. It is the local variation within this that emerges.

The short-range map for NDVI, Figure 4 c, looks like a mixture of the maps for R and I. However, there is more detail in the vegetated areas.

Long range

The long-range structures in the three maps, Figures 2 d, 3 d and 4 d, are very clear. This suggests that kriging with the long-range filter removes the local noise and shows the extent of the major ground cover classes. These maps are all different in the finer detail, but McKenna Hill and the roads stand out in all. Channels 2 and 3 both pick out the wet areas in the central southern part of the maps. The yellow areas on Figure 4 d for NDVI represent the wet areas, but they appear to be more extensive than in the other two maps.

Summary

There is considerable detail evident on the map of the long-range component, and from the point of view of environmental management at the broad scale these maps should enable a manager to identify areas for monitoring or more detailed study. The short-range maps could be of military value in that they show the amount of change in ground cover to be expected at the local scale. The difference in these scales is an order of magnitude. The local scale is around 150 m to 300 m and the long-range 1.5 km to 3 km. These maps also reflect the kinds of spatial scale of variation established from the image data in the first project and in the vegetation classes from the transects. Final interpretation of these results will depend on further information from TEC.

REFERENCES

Galli, A., Gerdil-Neuillet, F. & Dadou, C. 1984. Factorial kriging analysis: a substitute to spectral analysis of magnetic data. In: *Geostatistics for Natural Resource Characterization* (eds G. Verly *et al.*), pp 543-557. D. Reidel, Dordrecht.

Jaquet, O. 1989. Factorial kriging analysis applied to geological data from petroleum exploration. *Mathematical Geology*, **21**, 683-691.

Matheron, G. 1982. *Pour une analyse krigeante de données régionalisées.* Note N-732, Centre de Géostatistique, Ecole des Mines de Paris, Fontainebleau.

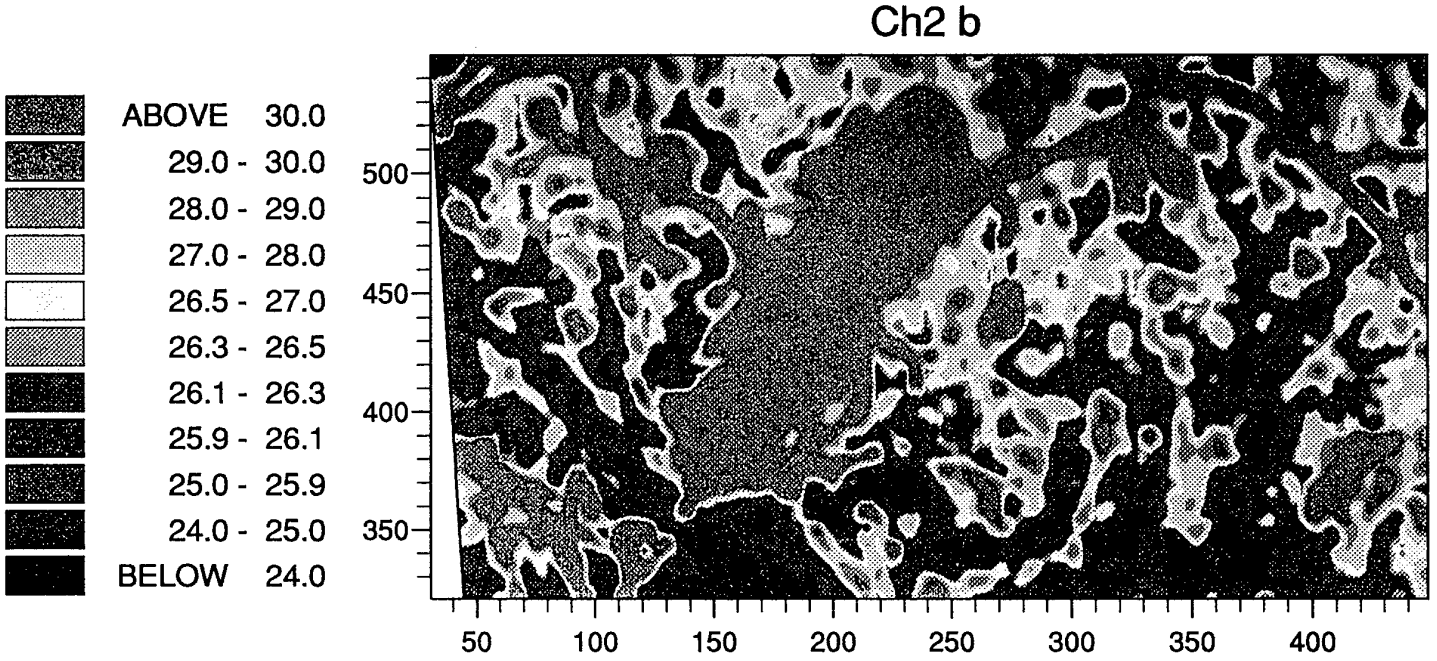

Figure 2 a. Map of ordinary kriged estimates for northern part of Fort Benning study area: Channel 2.

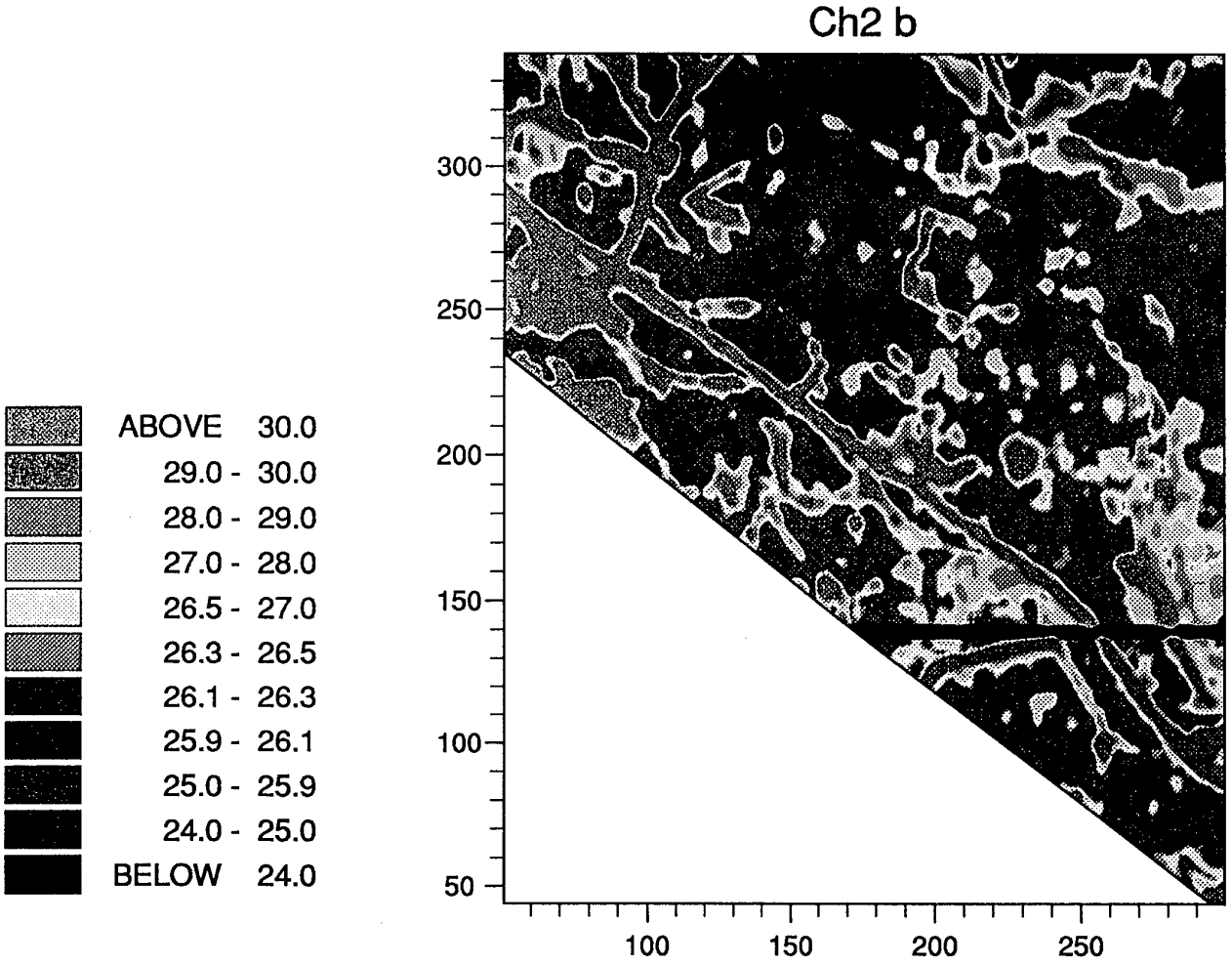

Figure 2 b. Map of ordinary kriged estimates for southern part of Fort Benning study area: Channel 2.

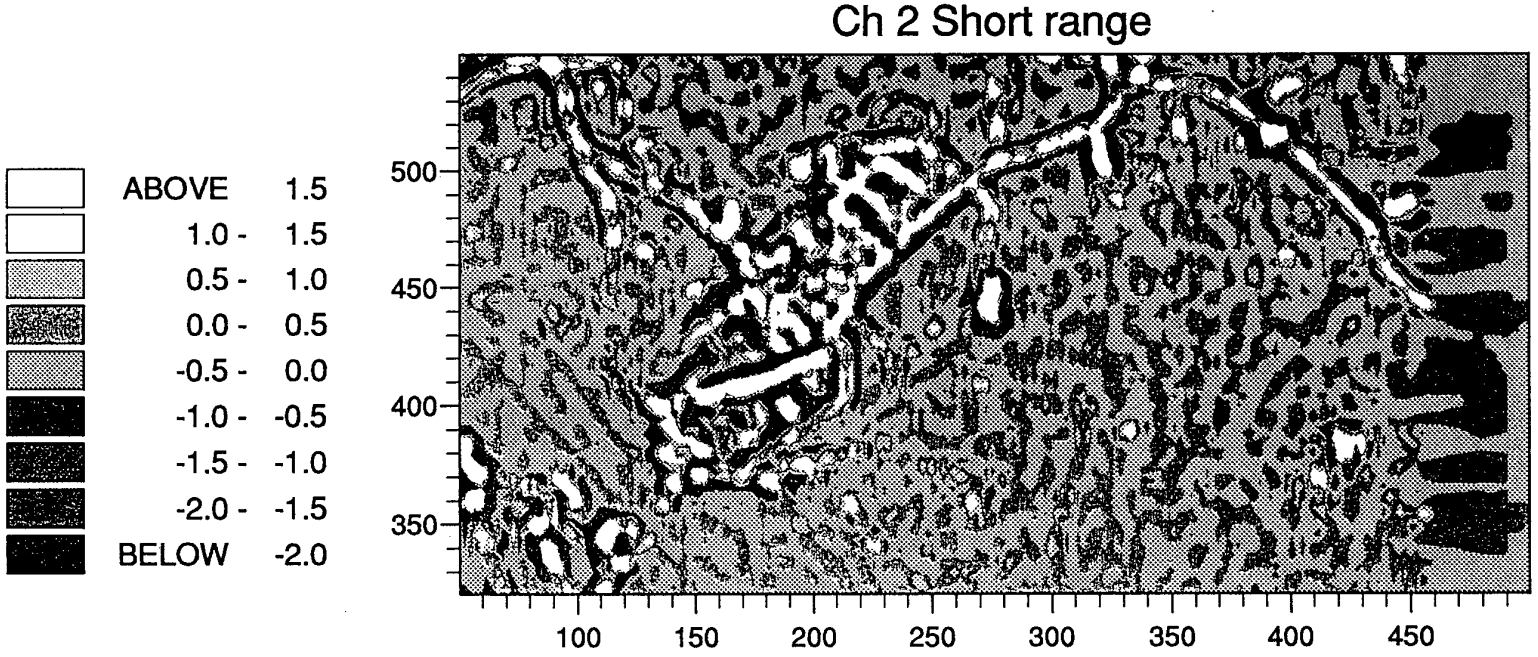

Figure 2 c. Map of short range kriged estimates after filtering for the northern part of Fort Benning study area: Channel 2.

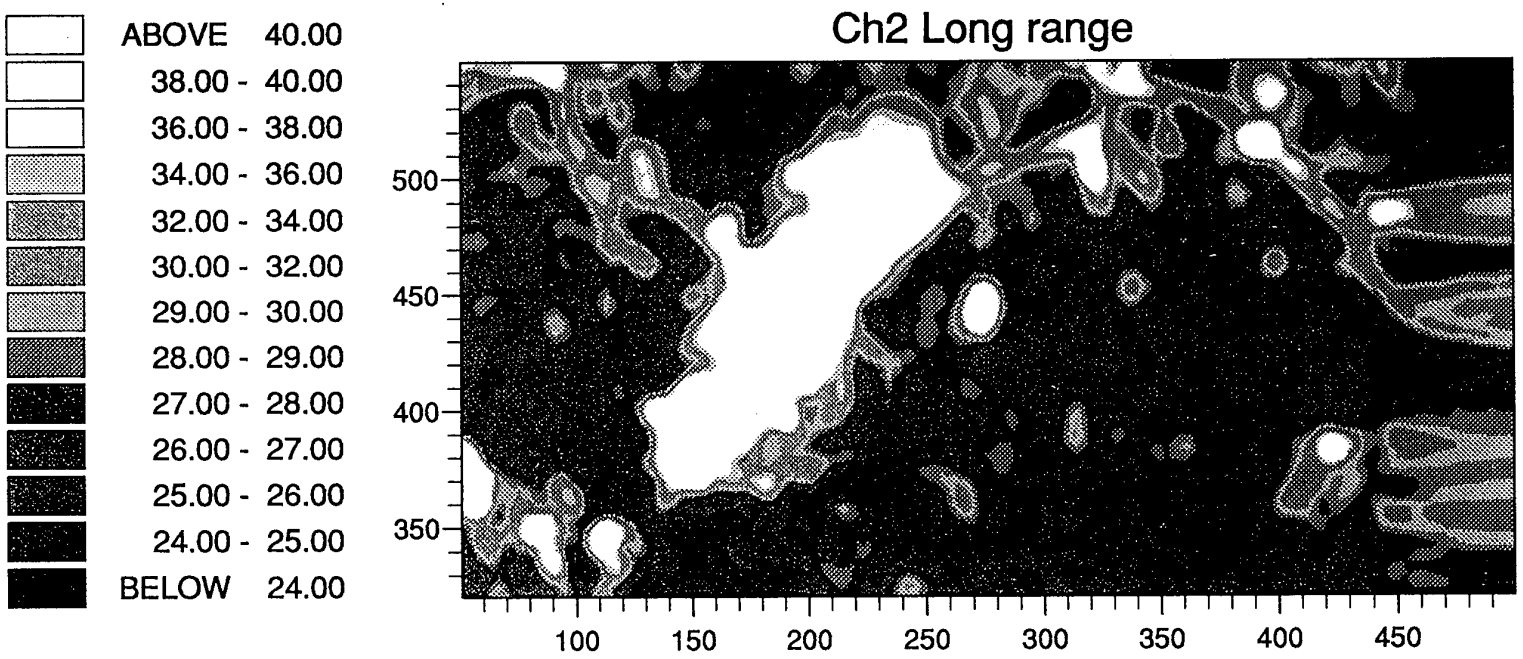

Figure 2 d. Map of long range kriged estimates after filtering for the northern part of Fort Benning study area: Channel 2.

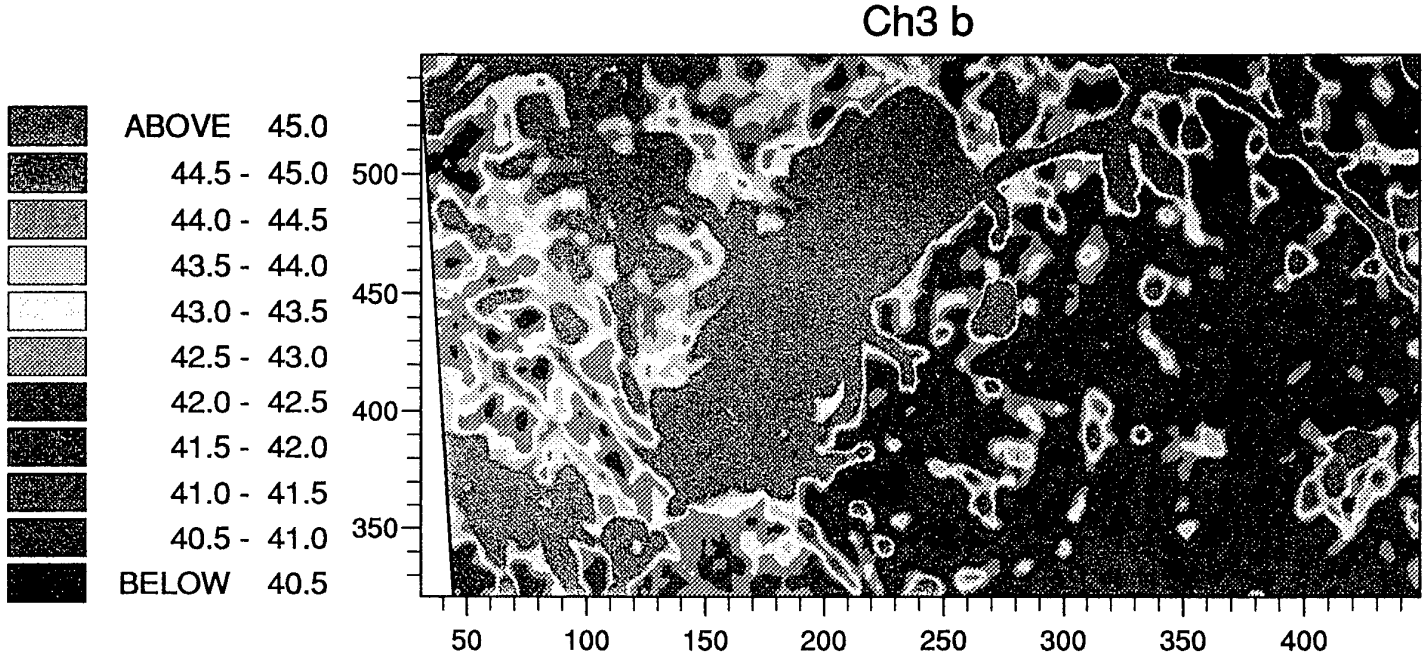

Figure 3 a. Map of ordinary kriged estimates for northern part of Fort Benning study area: Channel 3.

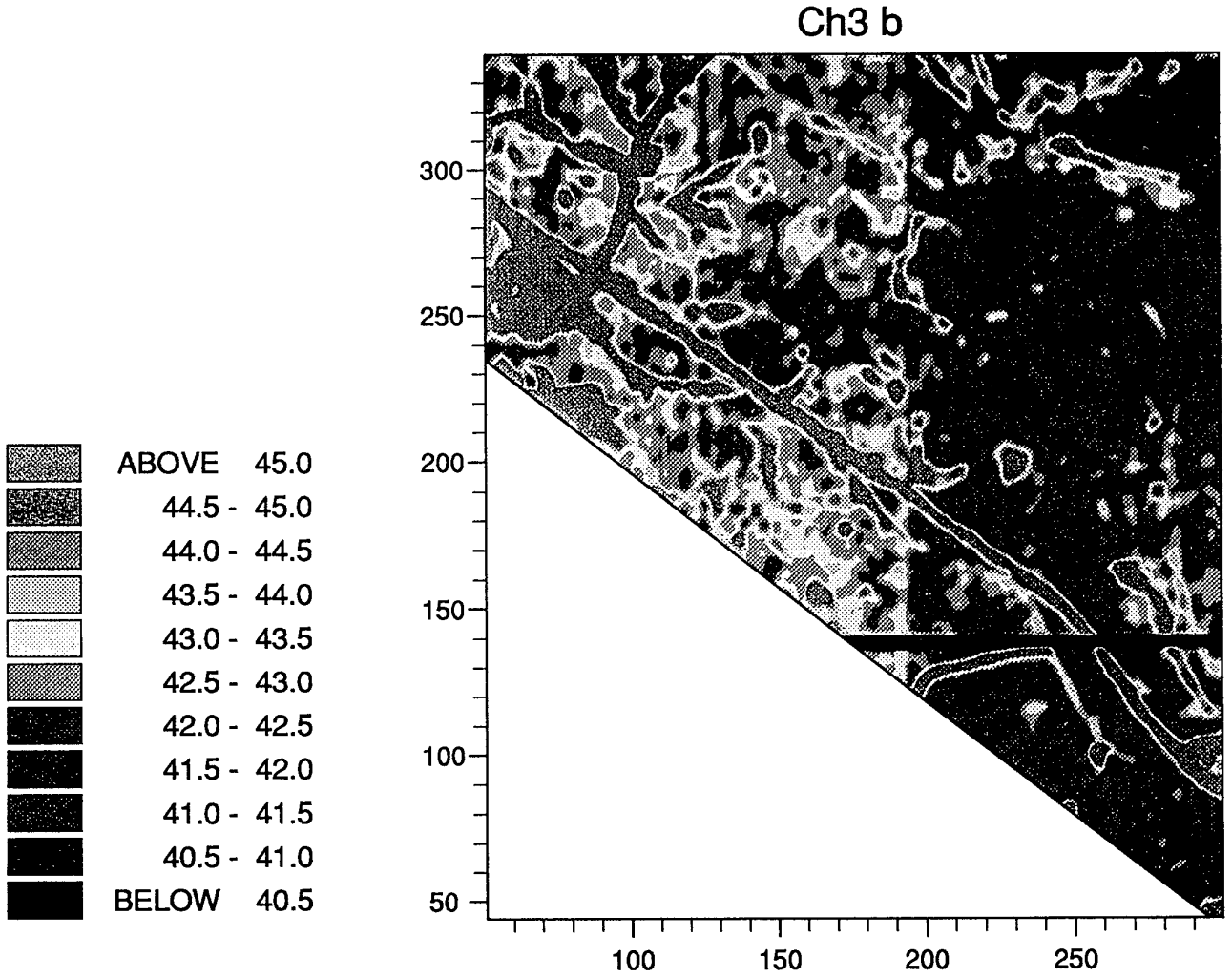

Figure 3 b. Map of ordinary kriged estimates for southern part of Fort Benning study area: Channel 3.

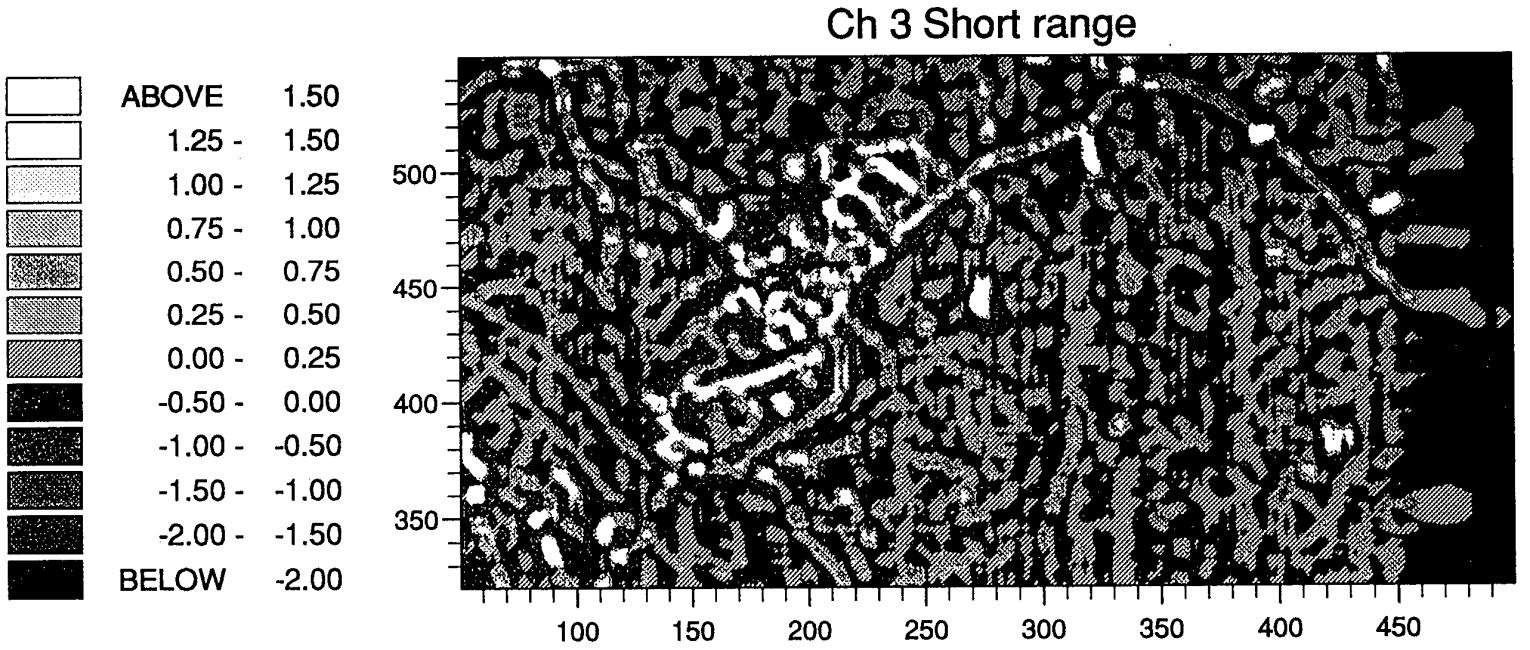

Figure 3 c. Map of short range kriged estimates after filtering for the northern part of Fort Benning study area: Channel 3.

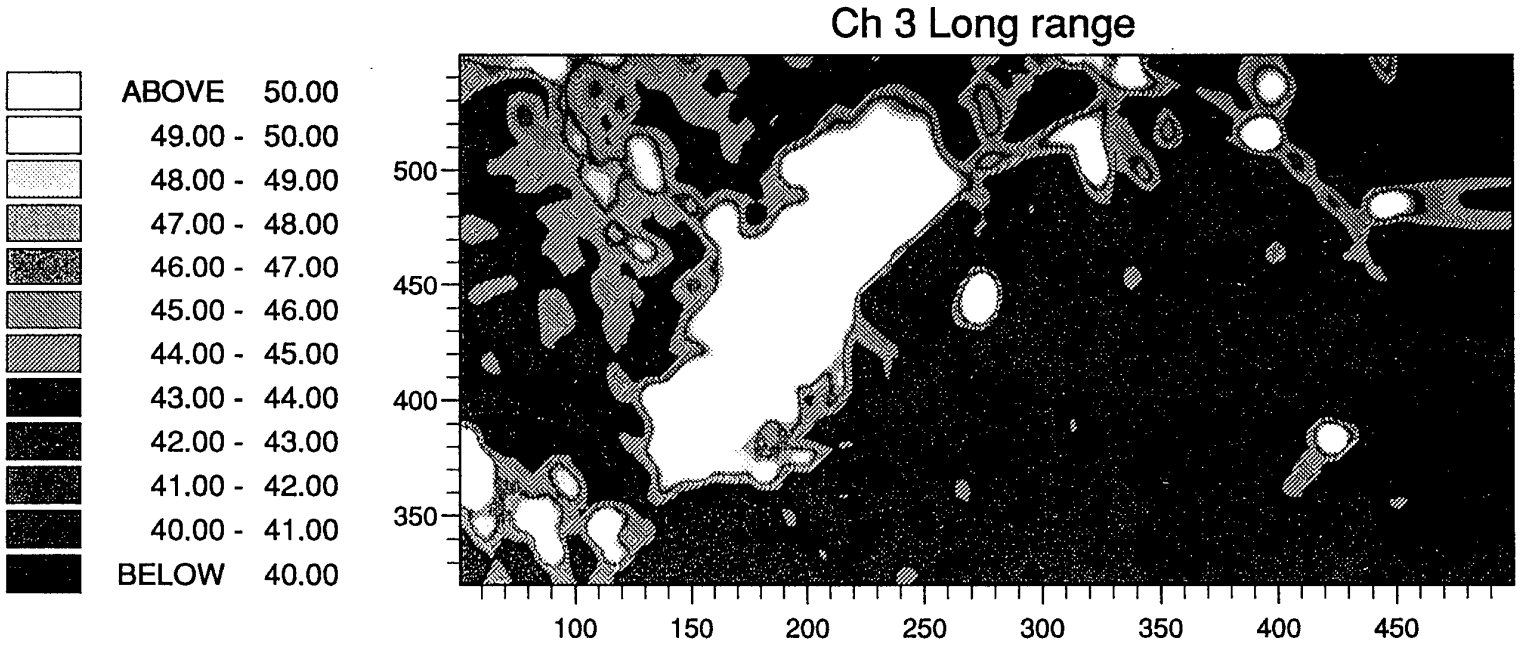

Figure 3 d. Map of long range kriged estimates after filtering for the northern part of Fort Benning study area: Channel 3.

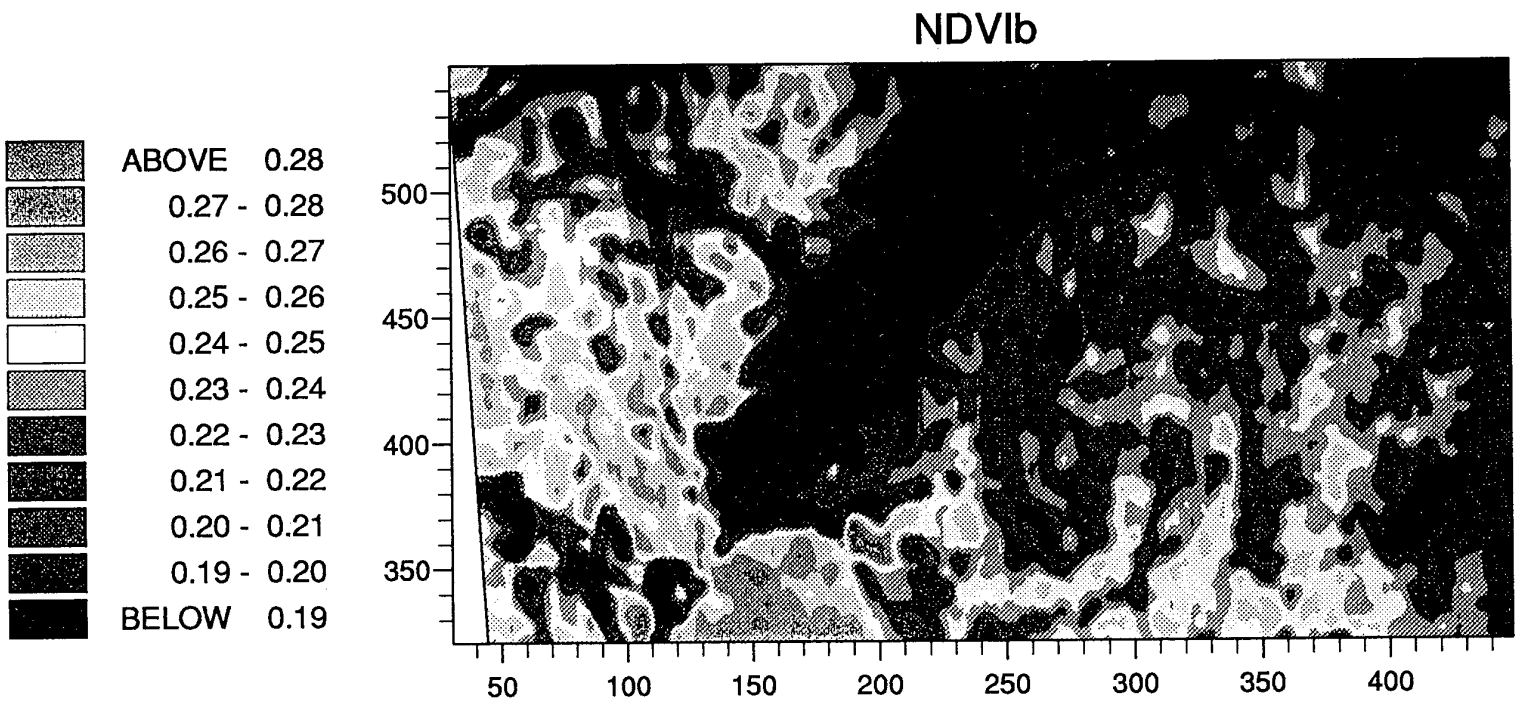

Figure 4 a. Map of ordinary kriged estimates for northern part of Fort Benning [illegible] NDVI

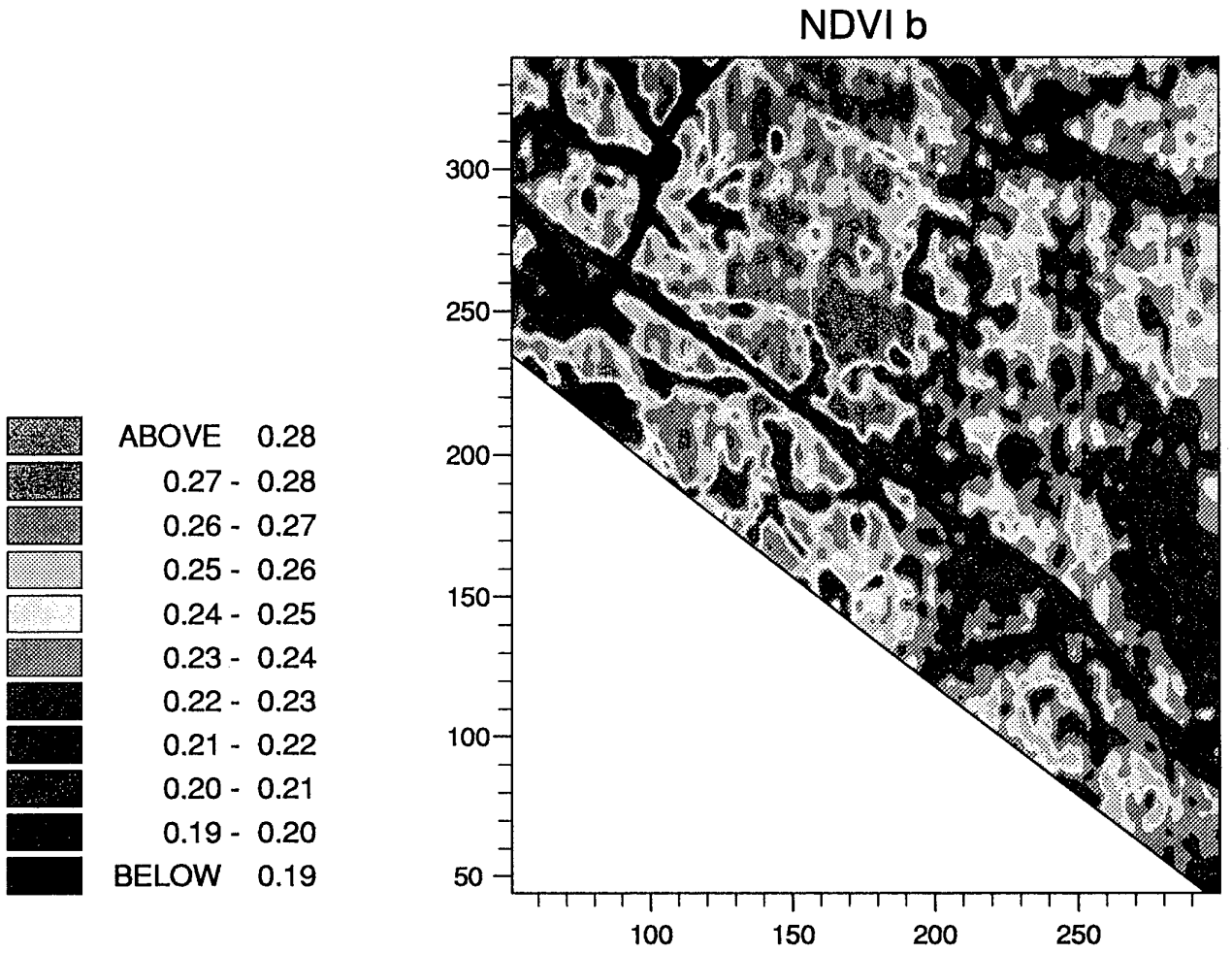

Figure 4b. Map of ordinary kriged estimates for southern part of Fort Benning study area: NDVI.

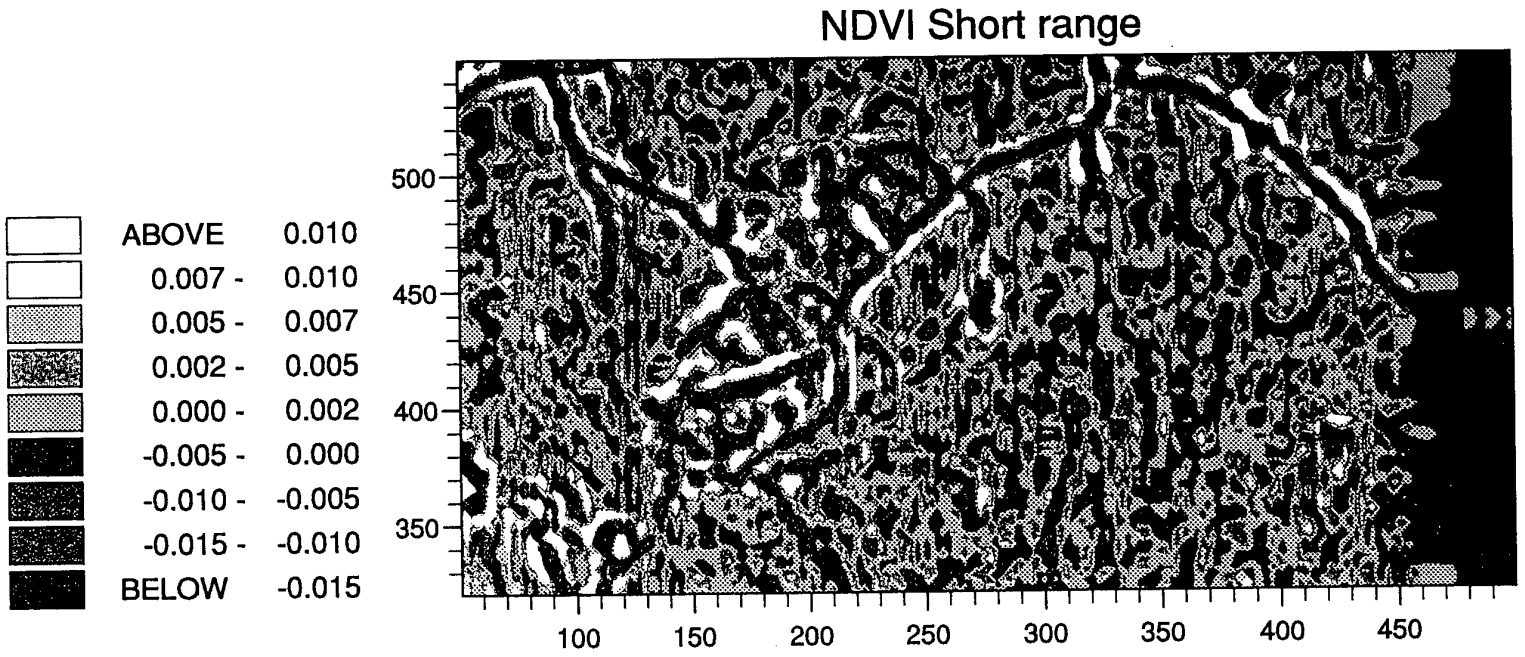

Figure 4 c. Map of short range kriged estimates after filtering for the northern part of Fort Benning study area: NDVI.

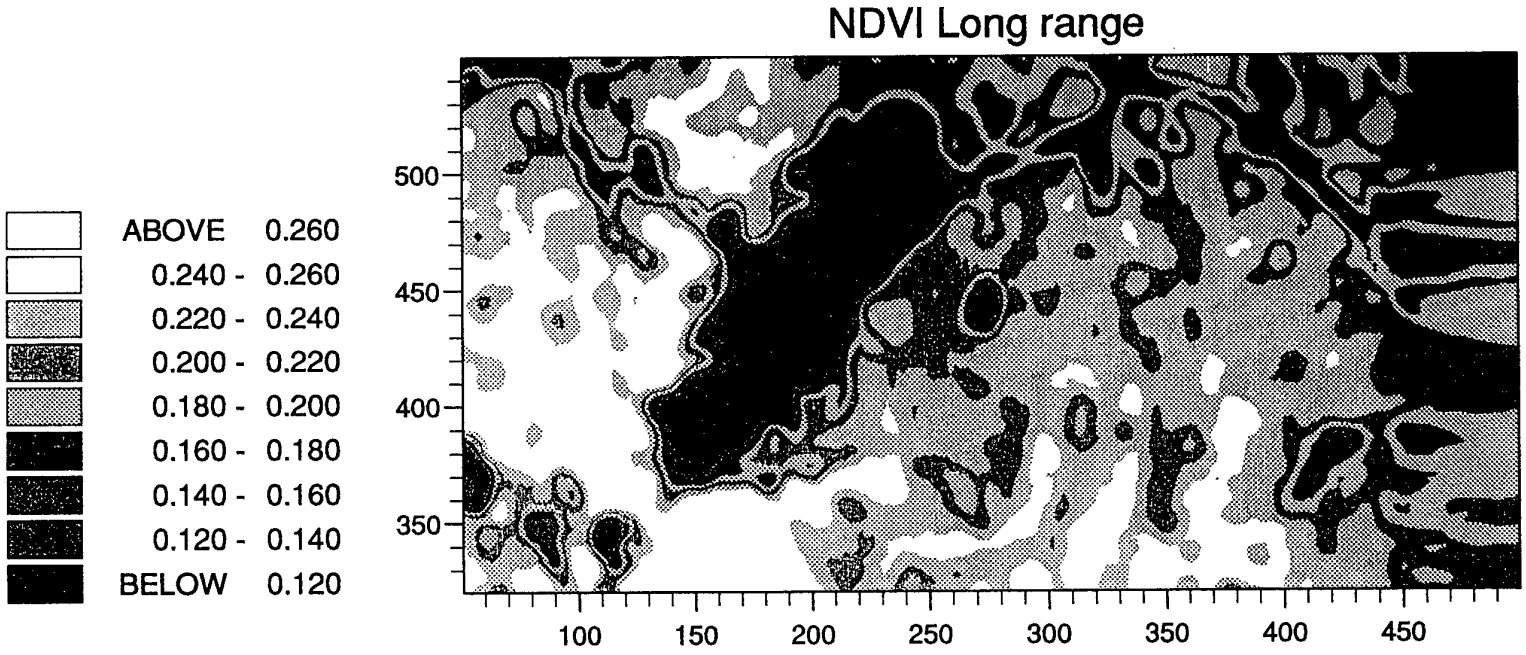

Figure 4 d. Map of long range kriged estimates after filtering for the northern part of Fort Benning study area: NDVI.